Check for updates

Energy Technology
Generation, Conversion, Storage, Distribution

Accepted Article

Title: Comparison and Scaling Effects of Rotational Micro-Generators using Electromagnetic and Piezoelectric Transduction

Authors: Hailing Fu and Eric M. Yeatman

This manuscript has been accepted after peer review and appears as an Accepted Article online prior to editing, proofing, and formal publication of the final Version of Record (VoR). This work is currently citable by using the Digital Object Identifier (DOI) given below. The VoR will be published online in Early View as soon as possible and may be different to this Accepted Article as a result of editing. Readers should obtain the VoR from the journal website shown below when it is published to ensure accuracy of information. The authors are responsible for the content of this Accepted Article.

To be cited as: *Energy Technol.* 10.1002/ente.201800151

Link to VoR: http://dx.doi.org/10.1002/ente.201800151

www.entechnol.de

WILEY-VCH

10.1002/ente.201800151

WILEY-VCH

FULL PAPER

Comparison and Scaling Effects of Rotational Micro-Generators using Electromagnetic and Piezoelectric Transduction

Hailing Fu*[a] and Eric M. Yeatman[b]

Abstract: Rotational energy is widely distributed or easily acquirable from other energy sources (fluid flow, machine operation or human motion) in many industrial and domestic scenarios. At small scales, power generation from such rotational ambient sources can enable many autonomous and self-reliant sensing applications. In this paper, three typical types of micro-generators (energy harvesters), namely electromagnetic (EMREHs), piezoelectric resonant (PRREHs) and piezoelectric non-resonant rotational energy harvesters (PNRREHs) are discussed and compared in terms of device dimensions and operation frequencies. Theoretical models are established for each type to calculate maximum achievable output power as a function of device dimension and operating frequency. Using these theoretical models, scaling laws are established for each type to estimate the achievable output. The EMREHs have a strong scaling effect both on device dimension (as L^5) and on operating frequency (as ω^2), whereas the PNRREHs are less so ($L^{2.5}\omega^{0.5}$). PRREHs have a narrow bandwidth as resonant harvesters, and are ideal for cases where the excitation frequency is constant. This study provides a guideline for selection and design of rotational energy harvesters (REH) when the device dimension and operating frequency are defined. The proposed scaling laws offer a convenient method to estimate the harvester performance for different dimensions and operating frequencies.

Introduction

Nowadays, electricity plays an indispensable role for almost every application in our daily life, ranging from domestic apparatus to industrial machines. Generally, electrical power is harvested by rotating generators using the electromagnetic transduction driven by different types of turbines.[1] This paradigm is ubiquitous and dominant in macro-scale generation systems to convert energy sources such as fluid flow, fossil fuels and nuclear power into electricity. However, at small-scales (e.g. <1 W), electromagnetic (EM) conversion is not the only transduction for rotational (kinetic) energy conversion. Several alternatives, such as piezoelectric, electrostatic, ferroelectric and triboelectric, which are inefficient at macro-scales, become effective and competitive.[2]

Micro-rotational energy harvesters based on different conversion mechanisms have been developed in the last two decades. The most straightforward solution is to miniaturize the conventional electromagnetic generators (EMG). A typical example is the electrical generators in kinetic wristwatches. First patented by Berney in 1976 [3], this technology has been developed and commercialized in many Seiko kinetic watches. The harvester generates rotation from human activities using an off-center rotor, and the motion is then amplified by gear trains before generating electricity using a micro-EMG.[4] Kinetron is another innovative organization specialized in micro kinetic systems, especially in EMG design.[5] These devices are designed for applications including wristwatches, mobile phones and pedal illumination systems. In watch applications, the claw-pole generator MG4.0 is the most commonly used design. A 14-pole Sm_2Co_{17} magnet and 1140 windings are integrated. The typical output power is 10 mW at 15,000 rpm (Φ4.0 × 2.2 mm). Donelan *et al* developed a bio-mechanical energy harvester generating electricity from walking with minimal user effort.[6] The harvester used the relative motion between upper and lower leg to generate rotation. After being amplified by a gear train, the energy was converted into electricity by an EMG. Similarly, Xie and Cai developed an in-shoe EM harvester.[7] The foot-strike motion was amplified by a trapezoidal slider, and then the linear motion was converted into rotation by a gear train. 1.2 W was extracted at 4 km/h walking speed. These devices are successful applications of EM rotational harvesters for wearable devices. However, gear trains are normally required; fabrication costs and system complexity need to be considered.

High rotational speeds are also achieved using other methods without using gear trains. Researchers from MIT conducted an extensive gas turbine program 10 years ago, in which they developed millimeter-scale gas turbine generators aiming to get 10-50 W from a less than 1 cm^3 device.[8] The generator was designed to operate at 1,000,000 rpm, and rotation was produced by a turbine with a compressor and a burner on a single chip. However, no experimental results of a whole device were reported. Other researchers focus more on the micro-turbogenerator subsystem using external flow energy. Peirs *et al* developed an axial-flow micro-turbine (Φ10 mm).[9] The harvester operated at 160,000 rpm with 16 W output. Holmes *et al* demonstrated an axial-flux EMG (Φ7.5 mm).[10] The device was tested at 30,000 rpm with 1.1 mW output. Arnold *et al* presented the optimization and characterization for a micro-EMG.[11] Different fabrication methods were discussed, and the presented device (Φ10 mm) produced 8 W at 305,000 rpm. Raisigel *et al* reported a Φ8 mm planar generator consisting of a permanent magnet rotor and a silicon stator with electroplated coils. [12] The harvester generated 5 W at 380,000 rpm and 14.6 mW at 58,000 rpm. These harvesters demonstrates promising harvesting capability at small scales (mW to W), but high rotational frequencies are inaccessible without gear trains or high-speed or high-pressure flows. These conditions are also infeasible in many practical applications.

Explorations have also been conducted by researchers to adopt the EM conversion in low-frequency rotation situations. Howey *et al* developed a Φ32 mm turbine for airflow energy harvesting. [13]

[a] Dr. H. Fu
Department of Aeronautics
Imperial College London
Exhibition Road, London, SW7 2AZ, UK
E-mail: h.fu14@imperial.ac.uk
[b] Prof E. M. Yeatman
Department of Electrical and Electronic Engineering
Imperial College London
Exhibition Road, London, SW7 2AZ, UK

Accepted Manuscript

This article is protected by copyright. All rights reserved.

This device can operate at air speeds down to 3 m/s and generated 4.3 mW at 10 m/s (corresponding to 4,000 rpm). Similarly, Zhao *et al* developed two air-driven planar EMGs with a low cut-in speed (1-2 m/s).[14] Kishore *et al* developed an airflow turbine with relatively large dimensions (the chord length is 75 mm) for wireless and portable devices with the cut-in speed of 1.7 m/s.[15] Romero-Ramirez developed micro-rotational EMGs for human motion.[16] Multiple pole pairs and increased coil turns were adopted to omit the use of gear trains.

In addition to EM conversion, piezoelectric (PE) conversion has also been widely adopted in rotational energy harvesting. Initially, researchers used rotational motion to induce a driving force close to the sinusoidal form for transducers, and the harvesters operate as resonant devices which have high output power at or close to resonance, but limited output at non-resonant conditions.[17] Priya *et al* demonstrated a piezoelectric windmill for airflow energy harvesting. In this design, airflow energy was first converted into rotation by a windmill.[18] An oscillating force was applied on the piezoelectric beams using direct impact generated by stoppers on a rotating host. A prototype with 12 bimorphs generated 10.2 mW at 6 Hz, but the direct impact is detrimental for the system stability and may cause material degradation.[19]

To avoid direct impacts, Khameneifar *et al* used the gravitational force of the tip mass on a PE beam to induce beam vibration from rotation.[20] The beam was mounted on a rotational host, whose rotational axis is perpendicular to the direction of gravity. A maximum power of 6.4 mW at 22 Hz was extracted. Similarly, Sadeqi *et al* presented a two-degree-of-freedom energy harvester for broadband rotational energy harvesting.[21] The harvester was a bimorph PE beam mounted on a flexible substructure. The fundamental frequency (8.8 Hz) and the second natural frequency (10.5 Hz) are close to each other, creating a wide operating bandwidth. Apart from the gravitational force, another excitation mechanism that is widely used in PE REHs is magnetic plucking. One successful implementation is the work from Karami *et al*.[22] A PE rotary transducer was integrated into a miniature wind turbine. Magnetic plucking was implemented by the magnetic force between magnets on piezoelectric beams' free ends and turbine blades. The magnetic force was alternating, creating a sinusoidal excitation force on the PE beams. 5 mW was extracted at 200 rpm. Similar designs with different design considerations, such as harvester configurations [23], magnet arrangements [24], operating conditions [25] and cut-in speed [26], were investigated.

In practice, the rotational speed is not constant in many situations, such as flow-induced rotation or machinery motion. Therefore, broadband harvesters are necessary, which cannot obtain from a PE resonant REH. Designs to overcome the bandwidth issue have been presented in the literature. Frequency up-conversion, a way to convert low-frequency random vibration into transducer's vibration at resonance, has been studied extensively to achieve broadband. In this mechanism, PE transducers are normally fixed on a static host, and plucked by impacts [27] or magnetic force [28]. Pozzi *et al* developed a knee-joint energy harvester to harness human motion.[29] The harvester used the relative motion between upper and lower leg to generate rotation. The PE beams on the inner hub fixed to the upper leg were plucked by the plectra on the outer ring mounted on the lower leg. An output power of 2.06 mW was extracted at 1 Hz walking speed. Also using mechanical impact, Yang *et al* presented a PE wind energy harvester.[30] 12 piezoelectric beams were installed at the circumference of the rotating fan, forming a polygon shape. Seven elastic balls were placed freely in the polygon structure as beam plectra. When the fan rotated, the elastic balls impacted the beams due to the inertial force or gravity.

Magnetic force is more attractive for system reliability due to its non-contact nature, and has been used in many broadband REHs. Pillatsch *et al* developed a scalable PE rotary harvester for human body excitation.[31] A cylindrical rotary proof mass was adopted to actuate an array of 8 PE beams via magnetic attraction. At a frequency of 2 Hz, a peak power output of 2.1 mW was obtained. However, the proof mass rolled on two linear guiding rails, which limited the travel range of the rotary motion. In a later version, they used an eccentric semi-circular mass to replace the cylindrical rotary proof mass. [32] The harvester collected a peak output power of 43 μW at 2 Hz and 20 m/s^2 with the beam dimensions of 19.5 ×1 × 0.37 mm^3. Inspired by this design, the magnetic plucking mechanism was applied into many other rotational scenarios, including miniature airflow turbines [33], rotating systems [34] and wearable devices [35].

Besides EM and PE conversion, there are other transductions, including electrostatic and triboelectric. Due to the application of electrets, external power is not needed for electrostatic harvesters. Therefore, this conversion mechanism is becoming popular in recent years. However, this mechanism is not yet widely adopted in rotational energy harvesting, although according to the current available reported devices [36], this method is promising due to its simplicity and high performance. Limitations could be the charge density of electrets and achievable capacitance. Triboelectric conversion is another possible option for rotational energy harvesting.[37] A few devices have been developed from Prof Wang's group at Georgia Tech.[38] These devices demonstrated possible solutions for kinetic energy harvesting. However, more consideration should be given on high output impedance, input requirements, mechanical reliability and output stability.

While rotating energy harvesters have been demonstrated using a number of transduction methods, there are currently no established principles by which to select the most suitable method in a particular application. This paper presents a theoretical study and comparison of three key types of REHs. Their theoretical achievable output power is analyzed. A comparison with specific structural parameters is presented to illustrate the general trend of harvester performance for different dimensions and operating frequencies. Scaling effects for each type are examined using the theoretical models. The results illustrate the differing sensitivity of the harvester types to device dimension and operating frequency. This work presents a detailed comparison of different REHs, and also provides a guidance for REH design when there are specific requirements for device dimensions and operating frequency.

Accepted Manuscript

This article is protected by copyright. All rights reserved.

Classification and Theoretical Modelling

Due to the fact that EM and PE transduction are the main methods used in REHs, the focus of this work is on the comparison of EM and PE harvesters. Based on the conversion mechanism and frequency dependence, REHs can be broadly classified into three categories, including electromagnetic (EMREH), piezoelectric resonant (PRREH) and piezoelectric non-resonant rotational energy harvesters (PNRREH), as shown in Fig. 1. For EMREHs, the rotating magnet leads to the variation of magnetic flux linkage in static coils, generating electricity. For PE harvesters in Fig. 1 (b) and (c), in both cases, each PE beam operates at its own resonant frequency. However, the harvester can be classified as resonant or non-resonant depending on the relation between the plucking of the beam by the rotating host and the beam's own vibration. The system is called resonant if the plucking frequency is synchronized with the beam vibration; otherwise it is non-resonant. For PRREHs, PE beams are excited by beam plectra, or exciters in an impact or a contactless manner. The excitation force on the beam is in an equivalent form of a sine wave which has the same frequency as the beam resonant frequency. For PNRREHs, the beam excitation mechanisms are the same as PRREHs, but the excitation frequency f_e of the rotating host is much lower than the resonant frequency f_r of the beams. Although the plucked beams oscillate at resonance after each plucking, the whole system operates in a non-resonant mode ($f_e \ll f_r$).

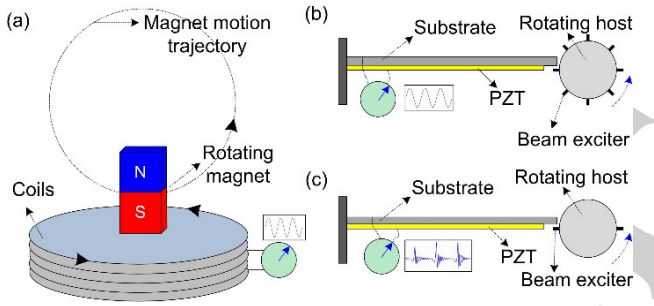

Figure 1. Schematic of three typical types of REHs. (a) Electromagnetic, (b) piezoelectric resonant and (c) Piezoelectric non-resonant.

Based on the design, EMREHs could also be resonant or non-resonant harvesters similar to Fig. 1 (b) and (c) if they incorporate a plucked, vibrating element. For example, by installing magnets on the cantilever beams in Fig.1 (b) or (c) and mounting stationary coils around these vibrating magnets, a resonant or non-resonant EMREH is obtained. This design has been extensively studied in vibration energy harvesting, where kinetic energy typically has the characteristics of high vibration frequency and low magnitude. In the vibration source case, a resonant or non-resonant EM harvester can be more suitable than a conventional EM generator design. However, the traditional EM generator design in the rotation source case is more effective – the vibrating elements are unnecessary (unlike in the PE case) and add unwanted complexity. Therefore, for EMREHs in this study, we mainly focus on harvesters based on conventional EM generator design.

Electromagnetic rotational energy harvesters

For EMREHs, there are generally two types of structures in terms of magnetic flux orientation, i.e. radial-flux and axial flux structures, as shown in Fig. 2. Radial-flux structures (Fig. 2(a)) are widely adopted in macro-scale power generation due to the high design flexibility and conversion performance. We consider geometries where a permanent-magnet rotor rotates inside the stationary armature windings; for simplicity we exclude generators with the permanent magnets in the stator, or with field windings rather than permanent magnets, as the scaling laws for these are similar. When device dimensions reduce to millimeter scale and below, radial-flux structures become undesirable due to limited magnet size, device fabrication difficulty (large coil area and reasonable coil turns and also structure compactness).

On the other hand, axial-flux structures have a good compatibility with micro-fabrication. The design and fabrication of coils and permanent magnets are relatively easy and flexible to achieve high flux linkage in coils and compactness in structure. Therefore, this design is widely used in applications where the device dimensions are on centimeter or millimeter scales. Power density is the priority in this design.[39] As shown in Fig. 2.(b), this type of harvester has a relatively high diameter-thickness aspect ratio (the "pancake" geometry). Both the rotor (permanent magnets) and stator (coils) are capable of utilizing the whole diameter.

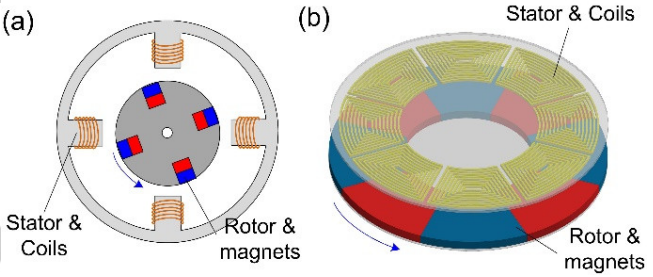

Figure 2. General EM generator designs: (a) radial-flux generator and (b) axial-flux generator.

For axial-flux generators, there are plenty of possible design configurations in terms of coil shapes, coil layers and rotor-stator number, as shown in Fig. 3. For coil fabrication, wire winding is

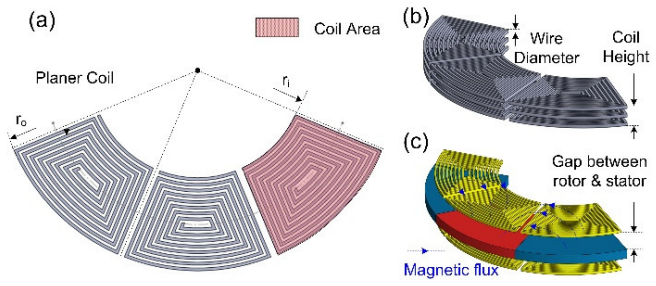

Figure 3. Design variables and possible configurations for axial-flux EMREHs: (a) planar coil design and key parameters, (b) multiple layer coil design (c) harvester with one rotor and two stators.

Accepted Manuscript

This article is protected by copyright. All rights reserved.

the typical method for conventional macro-scale EMGs. For EM harvesters, micro-fabrication technologies are available, including silicon-based fabrication and laser cutting. Multi-layer coils (Fig. 3(b)) can be fabricated to improve the output. Harvesters with one rotor and two stators are also possible (Fig. 3(c)). This type of coil shape is chosen in this study, as this shape has been optimized and used by several researchers in Ref [10], [13], [15] and [40]. For EMREHs, there are several key design considerations and practical limitations.

(1) Absolute value of magnetic flux density B and flux gradient. High B values require a high residual flux density (a reduced gap between magnets and coils). High magnetic flux gradient is necessary to achieve a high flux density variation (dB/dt) for a specific rotational frequency (increased output voltage).

(2) Coil area and coil turns. Axial-flux structures allow the coil to be planar, and a large portion of the cross-sectional area of devices can be filled, as shown in Fig. 3(b). Multi-layer coils can be integrated to alleviate the limitation of coil number in one layer, but the attenuation of magnetic field due to the increase of coil thickness should be considered.

(3) Output voltage. For EMGs, one significant issue is the low output voltage. Beeby *et al.* studied the effect of coil diameter and coil turns on output power and output voltage for vibrating harvesters.[41] For a certain coil volume, the increase of coil turns by decreasing coil diameter augments the output voltage, but the output power is essentially the same because of the increased impedance. Therefore, by optimizing the coil diameter and coil turns, the output voltage can be improved.

In order to understand the power generation capability of EMGs considering these key design limitations, a theoretical study is established based on the design in Fig. 2(b) and 3. Harvesters with one rotor and one stator are adopted. In this study, we assume the rotational source is not affected by the REH. Therefore, the damping effect on the source is not considered in characterizing EMREHs. However, such a damping effect should be considered in situations where the impact of the REH on the rotational sources is significant. For the topology introduced above, the maximum flux linkage is [10]

$$\Phi_0 = \beta_0 \cdot N_p \cdot N_t B_r A_c, \quad (1)$$

where B_r is the magnet remnant flux density, β_0 is a geometrical factor (<1) determined by coil-magnet arrangements, A_c is the average area enclosed by each coil, N_t is the number of turns for each spiral and N_p is the number of pole pairs.

Assuming the flux linkage Φ_0 varies with time sinusoidally, the rms output voltage can then be written as

$$V_{rms} = 1/\sqrt{2} \cdot N_p \omega \cdot \Phi_0, \quad (2)$$

where ω is the rotor angular speed. The theoretically achievable output power is then given by

$$P_{max} = V_{rms}^2/(4R_c), \quad (3)$$

where R_c is the coil internal resistance. The maximum achievable output power is obtained when the load resistance is equal to the internal coil resistance. This resistance can be calculated as [42]

$$R_c = \rho_c \cdot L_w/A_w = \pi\rho_c k_c (r_o^2 - r_i^2) t/A_w^2, \quad (4)$$

where ρ_c is the conductor resistivity, L_w is the total length of the wire, A_w is the cross section area of the wire, r_i and $r_o$are the coils' inner and outer radius, t is the thickness of the coils, and k_c is the fill factor. In wire wound transformers, copper fill factors in the range of 0.5-0.6 can be achieved.[43] For micro-fabricated coils, the fill factor will be lower, because the spacing needed for each turn is larger than that for wire-winding coils. The number of turns can be estimated using

$$N_t = L_w/L_m = k_c (r_o - r_i) t/A_w, \quad (5)$$

where L_m is the mean length of each turn.

More detailed theoretical modelling of general EM harvesters, including damping and nonlinear effects can be found in [44].

Piezoelectric resonant rotational energy harvesters

PE transduction has been extensively applied in vibration energy harvesting. These harvesters typically use the inertia of an over-hanged beam and tip mass to introduce vibration from base excitation. [45] However, in rotational situations, the host motion is generally low-frequency and continuous. Acceleration variation is not as significant as in the vibration case. PE harvesters excited by inertial force from rotation is not the typical design for REHs. Other mechanisms using tip excitation, such as magnetic plucking [46] or direct impact [47], are employed. The tip force generated from rotation plucks the piezoelectric beams, and electricity is collected from their subsequent oscillation.

Based on the frequency response, PE rotational harvesters can be classified into two categories: resonant and non-resonant, as shown in Fig. 1(b) and (c). For piezoelectric resonant rotational harvesters (PRREHs), the excitation force is in a harmonic form and multi-exciters are designed on the rotating host to amplify the effective rotational frequency. The plucking frequency generally matches the resonant frequency of the PE beams. Therefore, this type of harvester is suitable for conditions where the rotational speed is constant.

Two general designs for PRREHs are shown in Fig. 4, using direct impact or magnetic plucking. Other beam configurations are also possible in order to optimize the harvester performance. For magnetic plucking, the plucking force can be affected by environmental magnetic field or ambient ferromagnetic materials. Material selection should be considered in order to stabilize the performance. For the direct impact method, the constant and repetitive impacts on the brittle ceramic material is detrimental to system reliability. In addition, there are several practical limits for these harvesters as well.

(1) Maximum excitation force. This force is limited by the elastic limit of PE materials. Using materials with higher elastic limit or

Accepted Manuscript

This article is protected by copyright. All rights reserved.

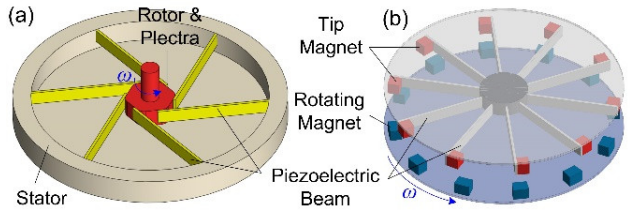

Figure 4. Possible implementation of PRREHs: (a) direct-impact actuated PRREH [18, 29] and (b) magnetic-force plucked PRREH [24, 32].

tapered beams could improve the maximum allowable force. In addition, appropriate protecting mechanisms, such as mechanical stoppers to limit the beam vibration amplitude, can be adopted to increase the system reliability.

(2) Material fatigue. PE materials are brittle. Long-term operation is an important factor in design. A safety factor should be included to avoid material failure.

(3) Number of PE beams. The number of beams affects the power conversion performance. It is ideal to integrate as many beams as possible to make the most of the space, but the complexity of the conditioning circuits should be considered. Synchronization methods which enable the beams to vibration in phase can potentially reduce the complication, and combining multiple power conditioning circuits in a single integrated circuit would be appropriate for a high volume product.

In order to evaluate the performance of PRREHs, a theoretical model is built. Assuming the tip excitation force is in harmonic form, it can be described as

$$F_{tip} = F_0 e^{j\omega t}, \tag{6}$$

where F_0 is the amplitude and ω is the plucking frequency. The amplitude F_0 is constrained by the maximum stress, i.e. tensile strength (σ_t), that the PE beam can withstand.

According to distributed-parameter theory, the dynamic equation of PE beams under tip excitation is [48]

$$YI\frac{\partial^4 v(x,t)}{\partial x^4} + c_s I\frac{\partial^5 v(x,t)}{\partial x^4 \partial t} + c_d\frac{\partial v(x,t)}{\partial t} + m\frac{\partial^2 v(x,t)}{\partial t^2}$$
$$-\vartheta V(t)\left[\frac{d\delta(x)}{dx} - \frac{d\delta(x-L)}{dx}\right] = F_{tip}\delta(x-L), \tag{7}$$

Where YI is the bending stiffness, $v(x,t)$ is the beam transverse deformation, c_s and c_d are the internal damping and the viscous deformation damping respectively, m is the mass per unit length, $\delta(x)$ is the Dirac delta function, ϑ is the PE coupling term in physical coordinates, $V(t)$ is the voltage across the PE beam, and L is the length of the beam. The transverse displacement can be obtained by separation of variables.

$$v(x,t) = \sum_{r=0}^{\infty}\varphi_r(x)\eta_r(t), \tag{8}$$

where $\varphi_r(x)$ is the mass-normalized eigenfunction of the r^{th} vibration mode, and $\eta_r(t)$ is the model mechanical coordinate expression. The mechanical equation can be further reduced to the modal coordinate by substituting Eq. (8) into Eq. (7) by multiplying $\varphi_r(L)$ and integrating over the beam length:

$$\frac{d^2\eta_r(t)}{dt^2} + 2\zeta_r\omega_r\frac{d\eta_r(t)}{dt} + \omega_r^2\eta_r(t) - \vartheta_r V(t) = \varphi_r(L)\cdot F_{tip}(T), \tag{9}$$

where ζ_r is the modal damping ratio and ω_r is the undamped modal frequency of the r^{th} mode shape. The damping ratios ζ_r are normally calculated using the logarithmic decrement method from experimentally measured beam displacement curves.[49] The deduction process from Eq. (7) to Eq. (9) can be found in Ref. [48]. For cantilever beams, the maximum stress σ_m happens at the fixed end of the beam on the surface farthest from the neutral axis. The stress should be kept lower than the tensile strength σ_T of the material to maintain the reliability of the device. The maximum stress can be calculated from

$$\sigma_m = \frac{E\cdot h}{2\rho} = \frac{E\cdot h}{2}\frac{\partial^2 v(x,t)}{\partial x^2}\Big|_{x=0} < \sigma_T, \tag{10}$$

where ρ is the bended beam curvature. In order to obtain maximum output power, a large input force is desirable, but the maximum stress generated by the input force should be lower than the tensile strength of the material. The maximum force F_{tip}^{max} can be calculated using Eq. (10). Normally, a safety margin (e.g. a safety ratio of 2) is set to limit the maximum stress lower than the limit to ensure the system reliability.

For PE transducers, an equivalent electric circuit is a current source in parallel with the internal capacitance. The electrical equation of PE beams can then be written as

$$C_p\frac{dV(t)}{dt} + \frac{V(t)}{R_l} + \sum_{r=1}^{\infty}\vartheta_r\frac{d\eta_r(t)}{dt} = 0, \tag{11}$$

where C_p is the internal capacitance, $\bar{e}_{31}$ is the PE constant, h_t is $(h_p + h_s)/2$, R_l is the load resistance and b and L are the beam width and length.

The maximum achievable average output power can be then calculated using

$$P_{max} = N_p\frac{\omega}{2\pi}\int_{t_0}^{t_0+\frac{2\pi}{\omega}}\frac{V^2(t)}{R_l}dt, \tag{12}$$

where N_p is the number of PE beams. The number of beams is determined by the beam configuration and the maximum bending displacement. In order to obtain the maximum output power, the optimal load resistance ($R_l = 1/(2\pi f_r C_p)$, where f_r is the beam resonant frequency) is used in Eq. (12). If the rotation frequency from the host is much lower than the resonant frequency of the beam, configurations that allow the beam to be longer should be adopted, and the number of exciters should be increased to ensure the harvester to operate at resonance.

Piezoelectric non-resonant rotational harvesters

For rotational energy sources, the operating frequency is typically inconstant. In many cases, such as car wheels and miniature air turbines, PRREHs are not suitable due to their narrow operating bandwidth. Therefore, non-resonant harvesters with wide operating bandwidth are desirable. The common topology for PNRREHs is illustrated in Fig. 1(c).

Accepted Manuscript

This article is protected by copyright. All rights reserved.

Compared with PRREHs, the number of exciters in PNRREHs is reduced, so that the excitation frequency (f_e) is much lower than the resonant frequency (f_r) of the PE beams, e.g. f_r>10f_e. The operating principle is indicated in Fig. 5. The beam is first plucked by exciters on the low frequency rotor, and then vibrates freely at its resonance. The beam oscillation has dampened before the next excitation comes. This mechanism is called frequency up-conversion, by which the low frequency rotation is converted to high-frequency beam vibration.

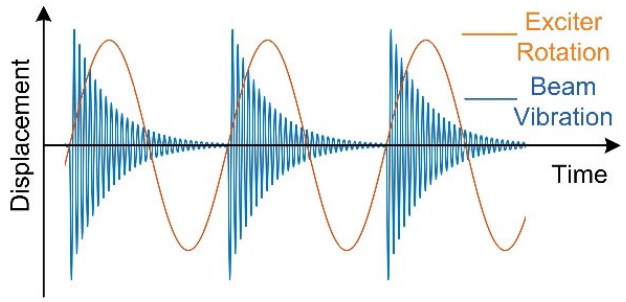

Figure 5. Displacement of exciter in the beam length direction and beam vibration, showing the operating principle of PNRREHs.

An advantage of PNRREHs is that the rotation and beam vibration are decoupled by this transient plucking for each excitation cycle. The kinetic energy is transferred to the beams during plucking. Once the energy is stored in the beam deformation, the beam is released from the plucking force, and the energy is gradually converted into electricity by PE transducers. By this mechanism, PNRREHs exhibit a wide operating bandwidth.

In order to evaluate the performance for different scales and operating conditions, the maximum achievable output power is estimated. As illustrated in Fig. 5, the beam vibration pattern in each excitation cycle is the damped free vibration. The transverse displacement of the beam at the free end ($x = L$) is

$$v(L,\ t) = A_0 e^{-\xi\omega_n t}\cos\left[\omega_d \cdot \mathrm{mod}\left(t, \frac{2\pi}{\omega}\right) - \theta_0\right] < \sigma_T, \quad (13)$$

where ξ is the beam total damping ratio and $\mathrm{mod}(x_1, x_2)$ is the function for the modulo operation.

Considering that the excitation frequency is much lower than the beam resonant frequency, the first vibration mode is, then, the dominant component. Therefore, in the following calculation, only the first mode is considered. The model mechanical coordinate expression $\eta_1(t)$ can then be written as

$$\eta_1(t) = B_0 e^{-\xi\omega_n t}\cos\left[\omega_d \cdot \mathrm{mod}\left(t, \frac{2\pi}{\omega}\right) - \theta_0\right] < B_0, \quad (14)$$

where B_0 is the initial amplitude.

From Eq. 9 and Eq. 10, the maximum stress can be rewritten as

$$\sigma_m = \frac{E\cdot h}{2}\frac{d\varphi_1^2(x)}{dx^2}\Big|_{x=0} \cdot \eta_1(t) \le \sigma_T. \quad (15)$$

The maximum initial amplitude of the model coordinate $\eta_1(t)$ to get the maximum output power can be denoted by

$$B_0^m = \frac{2\sigma_T}{E\cdot h}\left(\frac{d\varphi_1^2(x)}{dx^2}\Big|_{x=0}\right)^{-1}. \quad (16)$$

Therefore, the maximum vibrating condition for the PE beam is determined to get the maximum output power. The dynamics of the PNRREH can be obtained by solving Eq. 11 and Eq. 13. The maximum achievable output power can be calculated from Eq. 12.

Scaling Effect for Different Classifications

The achievable power of REHs is affected by device dimensions and by rotational frequency of the sources. In order to understand the performance variation for different classes, the scaling effects are examined. Considering that the aim of energy harvesting is to provide an alternative to conventional batteries, the dimensions of harvesters should be comparable to batteries. Hence, the scaling analysis focuses on the millimetre to centimetre scale. In addition, as the aim of this study is for low-frequency rotation sources, the rotational frequency is confined below 20 Hz (1200 rpm).

Electromagnetic rotational energy harvesters

For scaling analysis, the relative ratios of dimensions are retained. However, there are exceptions. The coil wire cross sectional area A_w of the coil wire and the magnets remnant flux density B_r are assumed to be constant. The minimum achievable wire diameter is a limiting factor in terms of fabrication. In order to achieve more coil turns, small wire diameter should be adopted. For flux density, if the magnet material and the relative gap between magnets and coil are constant, B_r is constant as well. The scaling effect can be examined based on the theoretical model build in Section 2.1.

According to Eq. (2) – (5), the scaling laws can be established. Assuming that the pole pair number N_p and the geometrical factor β, are the same for different scales, only A_c, r_o and r_i are affected by scaling, the scaling law can be built as

$$N_t \propto L^2,\ V_{rms} \propto L^4\omega, N_t \propto L^2, R_c \propto L^3 \text{ and } P_{max} \propto L^5\omega^2, \quad (17)$$

where L is the characteristic dimension and ω is the rotational frequency. This scaling law shows how the maximum achievable power is affected by both the device dimensions and the operating frequency. The device dimensions have a more significant impact (L^5). Since the scaling is more rapid than L^3, even the power density (P/L^3) is dropping rapidly with decreasing size.

The validity of the scaling laws can be examined by comparison to the theory from Trimmer.[50] In this paper, he derives that the magnetic force is proportional to L^3 between a wire with constant current and a permanent magnet, and the output power is proportional to the magnetic force ($P = F\dot{v} = F\omega r$). In our case, the current is inconstant; from Eq. (17), the current is proportional to $L\omega$, and r is proportional to L. If the varied current is considered, the same scaling law for dimension can be obtained.

In order to quantitatively study the scaling behaviour, a set of parameter values is given in Table 1. The rotor diameter D_r is the characteristic dimension, and other dimensions are dependent on this value. The diameter varies from 5 to 20 mm. The maximum achievable output power is estimated using Eq. (1) to (5). The result is illustrated in Fig. 6. As the diameter decreases from 20

Accepted Manuscript

This article is protected by copyright. All rights reserved.

mm to 10 mm, the output power drops from 220 μW to 7 μW at 5 Hz. A similar trend is illustrated for the rotational frequency. The output power is 1.26 mW at 12 Hz for the diameter of 20 mm, while the output power at 6 Hz is only 315 μW.

Table 1. Design parameters for electromagnetic rotational energy harvester

Symbol	Description	Values
D_r	Rotor diameter	5 – 20 mm
B_r	Remnant flux density	0.8 T
N_p	Number of pole pairs	5
r_i	Inner radius of coil annulus	0.25· D_r
r_o	Outer radius of coil annulus	0.5· D_r
t_h	Thickness of the device	0.2· D_r
G_{re}	Gap between magnets and coils	0.2· t_h
θ_0	Geometrical factor	0.02
ρ_{Cu}	Resistivity of copper	1.7 × 10^{-8}Ω·m
D_w	Diameter of coil wire	0.08 mm
k_{Cu}	Filling factor	0.6

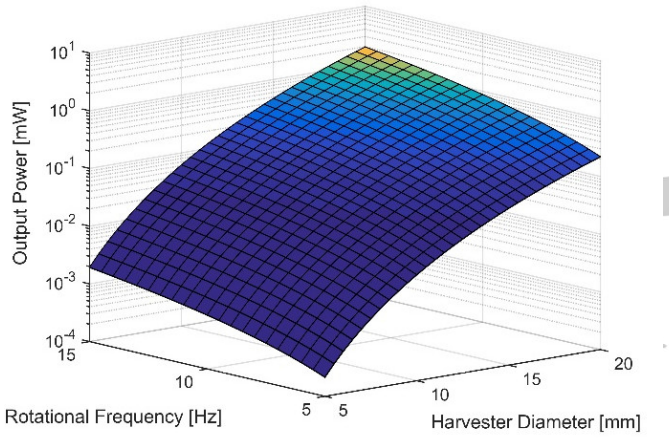

Figure 6. Output power of EMREHs as a function of diameter and frequency.

Piezoelectric resonant rotational energy harvesters

For PE harvesters, the system dynamics are more complex than EMREHs. There is no explicit solution for the output power as a function of device dimension and operating frequency. In order to study the scaling effects, the performance is calculated using several specific sets of harvester parameters. The scale law is then extracted from the calculated output. These multiple data sets are used to guarantee the universality of the scaling law.

Before studying the scaling law, one parameter needed to be investigated first is the dimension scaling effect on the mechanical damping of PE beams. This parameter is normally acquired from experiments, but it is impossible to test the values for all scales. The scaling effect on damping ratio has been studied by several researchers.[51] There are four main contributing factors for the damping forces, including air damping, squeeze effect, internal structural friction and support loss. The dominant factors at micro-scale are air damping and internal structural damping.[51b] The total mechanical damping ratio can be written as:[51a]

$$\xi_m = \xi_{a_b} + \xi_{a_m} + \xi_{in}, \quad (18)$$

where ξ_{a_b} and ξ_{a_b} are the air damping ratio of the beam and proof mass respectively and ξ_{in} is the internal structural damping ratio. For this type of harvester, there is typically no proof mass for the direct-impact excitation method (Fig. 4(a)), and the tip magnet can be regarded as the proof mass (Fig. 4(b)). The governing equations for these factors are shown below:

$$\xi_{a_b} = \frac{(3\mu\pi b + 0.75\pi\sqrt{2\rho_a\mu\omega}\cdot b^2)}{2\rho_a h b^2 \omega_n}, \quad (19)$$

$$\xi_{a_m} = \frac{(3\mu\pi a_m + 0.75\pi\sqrt{2\rho_a\mu\omega}\cdot a_m^2)}{2\rho_a c_m b_m^2 \omega_n} \text{ and} \quad (20)$$

$$\xi_{in} = \frac{m_b}{m_b + m_{pm}} \cdot \frac{\eta}{2}, \quad (21)$$

where μ is the viscosity of air (1.846 × 10^{-5} Pa·s), b and h are the beam width and thickness, a_m, b_m and c_m are is the length, width and height of the proof mass, ρ_a is the density of air, m_b and m_{pm} are the weight of the beam and proof mass and η is the structural damping coefficient determined by material properties.

From above equations, the scaling law for mechanical damping is not directly achievable. In order to study the scaling effect, a common piezoelectric ceramic beam, M1100 Johnson Matthey, is chosen to quantitatively study this effect. Main structural and material parameters for the model are summarized in Table 2. In this table, we assume the beam dimension scales with the diameter of the harvester. Different relative relations (α and β) will be studied to ensure the scaling law to be generic.

Table 2. Parameters for piezoelectric rotational energy harvesters: (a) resonant and (b) non-resonant.

Symbol	Description	Values
D_r	Rotor diameter	5 – 20 mm
L	Length of beam	D_r
b	Width of beam	α· D_r
h_p	Thickness of beam	β· D_r
$a_m \times b_m \times c_m$	Dimension of proof mass	(α × α × α)· D_r
ρ_p	Density of piezoelectric material	7700 kg/m³
ρ_s	Density of substrate material	1500 kg/m³
e_{31}	Piezoelectric constant	-22.2 V·m/N
d_{31}	Piezoelectric charge constant	-315 × 10^{-12} m/V
ε'_{r33}	Relative dielectric constant	4500
Y_s	Young's modulus of substrate	140 GPa
σ_T	Tensile Strength	80 MPa
(a) Resonant		
N_e	Number of exciters	*Variable*
N_b	Number of beams	Based on Vibration
(b) Non-resonant		
N_e	Number of exciters	*Variable*
N_b	Number of beams	Based on Vibration

As the structural damping coefficient η is constant for the same material operating in the same conditions, it can be calculated from one mechanical damping test, and then applied to other dimension scales. From Ref. [49], a damping ratio of 0.0175 was measured. According to Eq. (18) – (21), the structural damping coefficient can be calculated, and the value is 0.0355 Pa·s for a bimorph beam with carbon-fiber as substrate (M1100). This value is used in the following calculation for different scales.

Accepted Manuscript

This article is protected by copyright. All rights reserved.

Based on the above equations and structural parameters, the scaling effect on mechanical damping is calculated and shown in Fig. 7. As shown in Fig. 7(a), the internal structural damping is constant and the dominant factor in the range (5 - 20 mm) that we focus on. The air damping is much weaker and increases with the decrease of beam dimension. The total damping remains almost constant in this dimension range, and therefore this scaling effect can be ignored. In Fig. 7(b), different relative ratios of beam dimensions are considered, which demonstrates the universality of the scaling effect on mechanical damping in this range. The total mechanical damping in this dimension range (5 – 20 mm) can be regarded as constant.

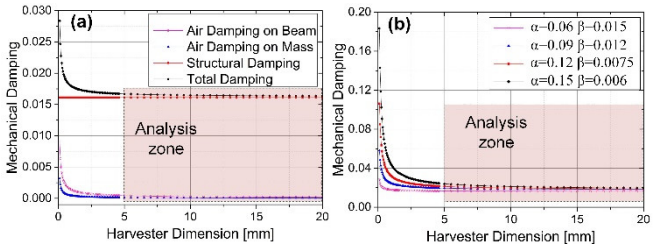

Figure 7. Scaling effect of harvester dimension on mechanical damping ratio. (a) Variation of damping factors again dimension for a particular beam dimension ratio α=0.06 and β=0.01 and (b) Scaling effect on total mechanical damping ratio for different beam relative dimension ratios.

Due to the complexity of the governing equations of PRREHs, the scaling laws for the maximum output power are not explicitly illustrated. In order to acquire these laws, the performance of for different scales and rotational frequencies is quantitatively studied first. The calculation is based on several specific data sets, as listed in Table 2. The power output for α=0.06 and β=0.015 is illustrated in Fig. 8(a). It is shown that PRREHs have a narrow bandwidth and therefore should operate in conditions where the rotational frequency is constant or varies in a narrow range.

For PRREHs, the resonant frequency is determined by the dimension of the transducers when the material parameters are fixed. Therefore, the rotational frequency is also a dependent variable of the harvester dimension. In order to examine the scaling effect on both the resonant frequency and the output power, these values are selected from Fig. 8(a) and depicted in Fig. 8(b) and (c). Different relative dimension ratios are adopted to examine the universality of the scaling law. Based on the calculation, the scaling laws for PRREHs can be expressed as

$$\omega_n \propto L^{-1} \text{ and } P_{max} \propto L^2, \quad (22)$$

where L is the characteristic linear dimension (D_r in this study).

Compared to EMREHs ($P_{max} \propto L^5$), PRREHs are less affected by the dimension scaling effect, to the extent that power density (P/L^3) actually increases with decreasing size. The bandwidth of PRREHs is limited due to the requirement of resonant vibration. In addition, in order to match the resonant frequency, multiple driving magnets are required to amplify the typically low rotational frequency. The implementation of driving magnets at small scale (e.g. μm scale) is difficult, especially when the resonant frequency ($\omega_n \propto L^{-1}$) is high.

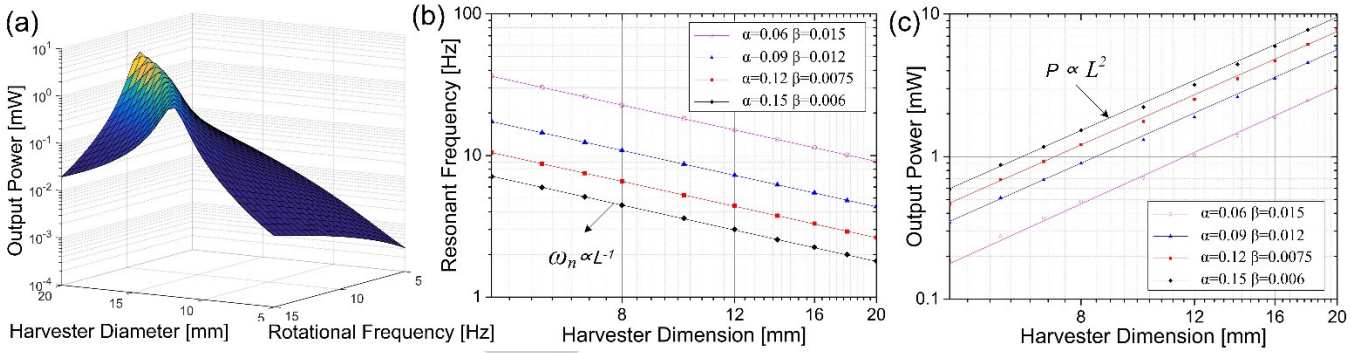

Figure 8. Scaling effect of harvester dimension on mechanical damping ratio. (a) Variation of damping factors again dimension for a particular beam dimension ratio α=0.06 and β=0.01 and (b) Scaling effect on total mechanical damping ratio for different beam relative dimension ratios.

Piezoelectric non-resonant rotational harvesters

For PNRREHs, the excitation frequency and the beam resonant frequency are decoupled by the frequency up-conversion method. Therefore, their operating bandwidth is wider, and the rotational frequency is not determined by the harvester dimension. The performance of PNRREHs is studied for different dimensions and rotational frequencies. The parameters used the same as those for PRREHs with a difference in the number of beam exciters. The output power as a function of harvester dimension and rotational frequency is illustrated in Fig. 9(a). The variation of output power has a similar trend to that of EMREHs. In order to understand the difference of the impact of the operation frequency and device dimension variation on the output power, the scaling law for output power of PNRREHs are studied for different harvester dimensions and rotational frequencies.

Fig. 9(b) depicts the output power of PNRREHs as a function of harvester diameter. The power is proportional to the harvester diameter (D_r) to the power of 2.5. Output power for different harvester diameters as a function of rotational frequency is shown in Fig. 9(c). The power is proportional to the rotational frequency to the power of 0.5. Different relative beam dimension ratios are investigated to ensure the stability of the scaling law on the output

Accepted Manuscript

This article is protected by copyright. All rights reserved.

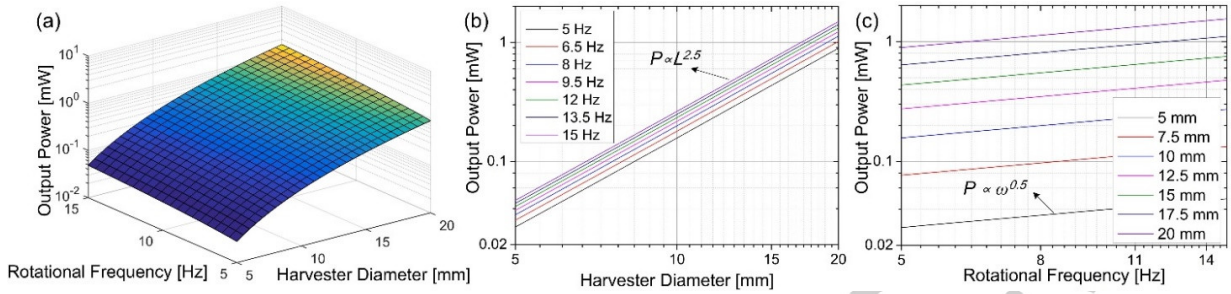

Figure 9. Output power and scaling laws of PNRREHs. (a) Output power versus harvester diameter and rotational frequency, (b) scaling effect of harvester dimension and (c) scaling effect of rotational frequency (α=0.06 and β=0.015.

of PNRREHs, as illustrated in Fig. 10. Logarithmic coordinates are adopted for each axis, and the output power for different beam relative dimension ratios is parallel to each other, so the stability of the scaling law is verified. Based on the above analysis, the scaling law for PNRREHs is

$$P_{max} \propto L^{2.5}\omega^{0.5}, \quad (23)$$

where L is the characteristic linear dimension (D_r) and ω is the driving rotational frequency.

Table 3. Scaling effect of harvester dimension and rotational frequency on the output power of three types of rotational energy harvesters.

Output Power	Device Dimension (L)	Rotational Frequency (ω)
P_{EMREH}	L^5	ω^2
P_{PRREH} [a]	L^2	-
P_{PNRREH}	$L^{2.5}$	$\omega^{0.5}$

[a] PRREHs are normally designed to operate at resonance, and ω_n is proportional to L^{-1}.

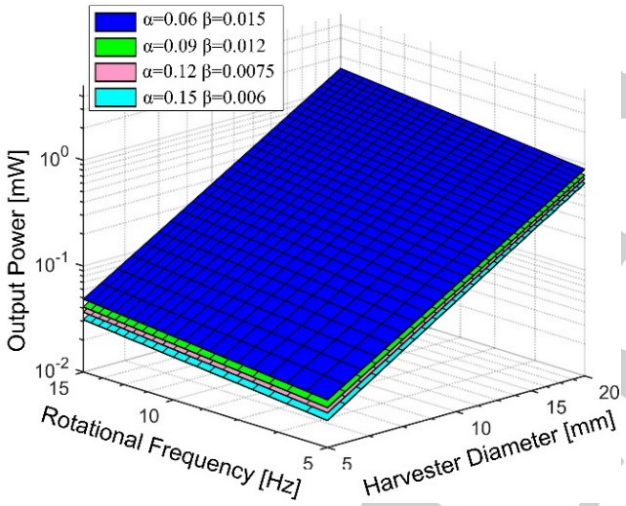

Figure 10. Output power versus rotational frequency and harvester dimension for different relative dimension ratios of PNRREHs.

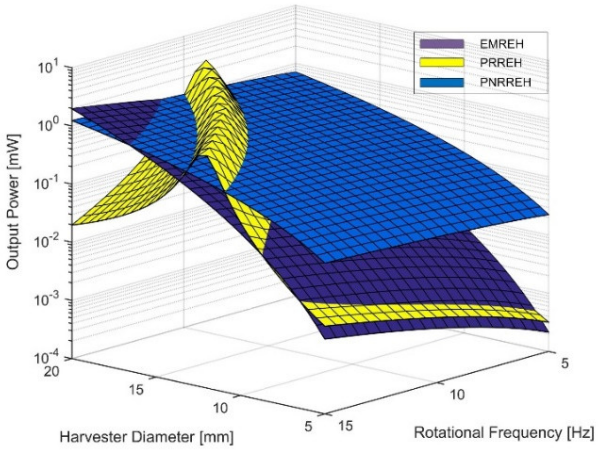

Figure 11. Performance comparison of three types of harvesters for different harvester dimensions and rotational frequencies. The results from Fig.6, Fig.8 (a) and Fig. 9 (a) are combined.

Hereto, the scaling effects in terms of harvester dimension and rotational frequency on the output power of three types of REHs are discussed, as summarized in Table 3. These scaling laws can be used to estimate the performance of the same harvester design on different dimension and operating frequency scales. In addition, from the scaling laws we can find that the performance of EMREHs is more sensitive to device dimension and rotational frequency than the other types. PRREHs are designed to operate at resonance, and the scaling effect of harvester dimension has the lowest influence on the output power. However, due to the narrow bandwidth, these harvesters are not suitable for conditions where rotational frequency varies in a wide range. For PNRREHs, the scaling effect of both parameters is relatively low. Therefore, these harvesters are, in principle, more feasible for small-scale and low-frequency applications.

In Fig. 11, the performance of the three types of harvesters are compared using the specific data sets discussed above. Due to the fact that the calculation is conducted using specific design parameters, the figure shows the general trend of performance variations for different types. Given that there are different designs and material properties available [52], the boundaries shown in this figure cannot be used as a universal criteria for determining the best design for a particular dimension and frequency region.

However, we can still find some useful guidelines for other researchers for rotational energy harvester design. PRREHs have the dominant performance over a narrow bandwidth at resonance. When harvester dimension and rotational frequency increase, the performance of EMREHs increases dramatically. This explains

Accepted Manuscript

This article is protected by copyright. All rights reserved.

the overwhelming application of electromagnetic conversion at macro scale. However, the performance decreases rapidly with the decrease of dimension and frequency. Compared to EMREHs, PNRREHs has a significant advantage for low-frequency and small-scale conditions, even when the operating frequency varies in a wide range. For the specific data set used in Fig. 11, EMREHs are ideal to operate for device diameter larger than 10 mm and driving rotational frequency larger than 10 Hz. The advantage of PNRREHs becomes significant when the device diameter is less than 10 mm and the rotational frequency is below 10 Hz, and the output power is generally below 1 mW. This also indicates that for rotational energy harvesting at small scale and low frequency, PNRREHs are desirable.

Conclusions

As an essential enabler for pervasive and autonomous wireless sensing, rotational energy harvesting has drawn great attention in recent years. In this paper, we present a theoretical comparison of three key types of rotational energy harvesters, including electromagnetic (EMREH), piezoelectric resonant (PRREH) and piezoelectric non-resonant (PNRREH). Theoretical models were established for each type considering the device dimension and operating frequency. Power generation capabilities are examined using specific design parameters to illustrate the performance variations in terms of device dimension and operating frequency.

Scaling laws for device dimension and operating frequency on harvester output power are investigated based on the theoretical analysis. EMREHs have strong dimension and frequency scaling effects ($P \propto L^5\omega^2$) compared to the others, whereas PNRREHs are relatively insensitive to the device dimension and frequency variation ($P \propto L^{2.5}\omega^{0.5}$). PRREHs are ideal to operate at resonant (these harvesters have a narrow operating bandwidth), and have the lowest dimension scaling effect ($P \propto L^2$).

Based on the comparison of the output power for the three types, the ideal operating zone for each type is identified using several specific optimized sets of design parameters. EMREHs are desirable to operate at high operating frequency at macro-scale (e.g. > 10 mm & > 10 Hz). PNRREHs are ideal for micro-scale cases operating at low frequency (e.g. < 10 mm & < 10 Hz). RRREHs are designed to operate at resonance. The operating frequency needs to be constant or vary in a narrow range. Further optimization, such as coil optimization for EM harvester or beam arrangement optimization for PE harvesters, can be conducted to input the performance and ideal operating range of each type.

The theoretical comparison and scaling laws established in this paper provides a guideline for selection and design of rotational energy harvesters with specific device dimension and operating frequency requirements. The proposed scaling law also offers a handy method to estimate harvester performance for different device dimensions and operating frequencies.

Acknowledgements

The work is supported by the China Scholarship Council (CSC) and the Department of Electrical and Electronic Engineering, Imperial College London.

Keywords: Rotational energy harvesting • Electromagnetic • Piezoelectric • Scaling effect • Non-resonant

[1] J. B. Ekanayake, L. Holdsworth, X. Wu, N. Jenkins, *IEEE Transactions on Power Systems* **2003**, *18*, 803-809.

[2] (a) K. Uchino, Piezoelectric Energy Harvesting Systems – Essentials to Successful Developments, *Energy Technology*, **2017**, online; (b) G. Zhang, M. Li, H. Li, Q. Wang, S. Jiang, Harvesting Energy from Human Activity: Ferroelectric Energy Harvesters for Portable, Implantable and Biomedical Electronics, *Energy Technology*, **2017**, online.

[3] J. C. Berney, Watch movement driven by a spring and regulated by an electronic circuit. Google Patents: **1976**.

[4] Seiko Kinetic Watches, Spring Drive. http://www.seiko.co.uk/discover-seiko/technology/spring-drive.

[5] Kinetron SMART ENERGY HARVESTERS. https://www.kinetron.eu/.

[6] J. M. Donelan, Q. Li, V. Naing, J. Hoffer, D. Weber, A. D. Kuo, *Science* **2008**, *319*, 807-810.

[7] L. Xie, M. Cai, *IEEE/ASME Transactions on Mechatronics* **2015**, *20*, 3264-3268.

[8] (a) A. H. Epstein, *ASME Turbo Expo 2003, collocated with the 2003 International Joint Power Generation Conference, American Society of Mechanical Engineers* **2003**, 669-696; (b) A. Mehra, X. Zhang, A. A. Ayón, I. A. Waitz, M. A. Schmidt, C. M. Spadaccini, *Journal of Microelectromechanical systems* **2000**, *9*, 517-527.

[9] J. Peirs, D. Reynaerts, F. Verplaetsen, *Sensors and Actuators A: Physical* **2004**, *113*, 86-93.

[10] A. S. Holmes, G. Hong, K. R. Pullen, *Journal of microelectromechanical systems* **2005**, *14*, 54-62.

[11] D. P. Arnold, F. Herrault, I. Zana, P. Galle, J.-W. Park, S. Das, J. H. Lang, M. G. Allen, *Journal of micromechanics and microengineering* **2006**, 16, S290.

[12] H. Raisigel, O. Cugat, J. Delamare, *Sensors and Actuators A: Physical* **2006**, *130*, 438-444.

[13] D. A. Howey, A. Bansal, A. S. Holmes, *Smart Materials and Structures* **2011**, *20*, 085021.

[14] J. Zhao, G. Shi, L. Du, *Energies* **2015**, *8*, 11755-11769.

[15] R. A. Kishore, A. Marin, S. Priya, *Energy Harvesting and Systems* **2014**, *1*, 27-43.

[16] E. Romero-Ramirez, Michigan Technological University, Thesis, **2010**.

[17] (a) T. Kumar, R. Kumar, V. S. Chauhan, J. Twiefel, *Energy Technology*, **2015**, *3*, 1243–1249; (b) H. Fu H, E. M. Yeatman, *Smart Materials and Structures,* **2018**, in press.

[18] S. Priya, C.-T. Chen, D. Fye, J. Zahnd, *Japanese journal of applied physics* **2004**, *44*, L104.

[19] P. Pillatsch, B. Xiao, N. Shashoua, H. Gramling, E. M. Yeatman, P. Wright, *Smart Materials and Structures* **2017**, *26*, 035046.

[20] F. Khameneifar, S. Arzanpour, M. Moallem, *IEEE/ASME Transactions on Mechatronics* **2013**, *18*, 1527-1534.

[21] S. Sadeqi, S. Arzanpour, K. H. Hajikolaei, *IEEE/ASME Transactions on Mechatronics* **2015**, *20*, 2085-2094.

[22] M. A. Karami, J. R. Farmer, D. J. Inman, *Renewable energy* **2013**, *50*, 977-987.

[23] R. A. Kishore, D. Vučković, S. Priya, *Ferroelectrics* **2014**, *460*, 98-107.

[24] N. Rezaei-Hosseinabadi, A. Tabesh, R. Dehghani, A. Aghili, *IEEE Transactions on Industrial Electronics* **2015**, *62*, 3576-3583.

[25] J. Kan, C. Fan, S. Wang, Z. Zhang, J. Wen, L. Huang, *Renewable Energy* **2016**, *97*, 210-217.

[26] D. Avirovik, R. Kishore, S. Bressers, D. Inman, S. Priya, *Integrated Ferroelectrics* **2015**, *159*, 1-13.

[27] (a) R. Lockhart, P. Janphuang, D. Briand, N. F. de Rooij, *Micro Electro Mechanical Systems (MEMS), 2014 IEEE 27th International Conference on, IEEE*: **2014**, 370-373; (b) P. Janphuang, R. A. Lockhart, D. Isarakorn,

Accepted Manuscript

This article is protected by copyright. All rights reserved.

S. Henein, D. Briand, N. F. de Rooij, *Journal of Microelectromechanical Systems* **2015**, *24*, 742-754.

[28] (a) R. Ramezanpour, H. Nahvi, S.Ziaei-Rad, *Journal of Vibration and Acoustics* **2017**, *139*, 011016; (b) H. Fu, E.M. Yeatman, *Mechanical Systems and Signal Processing*, **2018**, in press.

[29] M. Pozzi, M. S. Aung, M. Zhu, R. K. Jones, J. Y. Goulermas, *Smart Materials and Structures* **2012**, *21*, 075023.

[30] Y. Yang, Q. Shen, J. Jin, Y. Wang, W. Qian, D. Yuan, *Applied Physics Letters* **2014**, *105*, 053901.

[31] P. Pillatsch, E. M. Yeatman, A. S. Holmes, *Smart Materials and Structures* **2012**, *21*, 115018.

[32] P. Pillatsch, E. M. Yeatman, A. S. Holmes, *Sensors and Actuators A: Physical* **2014**, *206*, 178-185.

[33] (a) H. Fu, E. M. Yeatman, *Journal of Physics: Conference Series, IOP Publishing* **2015**, 012058; (b) H. Fu, E. M. Yeatman, *Applied Physics Letters* **2015**, *107*, 243905.

[34] W.-H. Wu, K.-C. Kuo, Y.-H. Lin, Y.-C. Tsai, *Microelectronic Engineering* **2018**, *191*, 16-19.

[35] (a) T. Xue, S. Roundy, *Sensors and Actuators A: Physical* **2017**, *253*, 101-111; (b) H. Fu, G. Chen, N. Bai, *Sensors* **2018**, *18*, 804.

[36] (a) J. Nakano, K. Komori, Y. Hattori, Y. Suzuki, *Journal of Physics: Conference Series, IOP Publishing* **2015**, 012052; (b) M. Perez, S. Boisseau, P. Gasnier, J. Willemin, M. Geisler, J. Reboud, *Smart materials and structures* **2016**, *25*, 045015.

[37] N. Kaur, K. Pal, A comprehensive review on Triboelectric Nanogenerator as a mechanical energy harvester, *Energy Technology* **2017**, online.

[38] (a) L. Lin, S. Wang, Y. Xie, Q. Jing, S. Niu, Y. Hu, Z. L. Wang, *Nano letters* **2013**, *13*, 2916-2923; (b) L. Lin, S. Wang, S. Niu, C. Liu, Y. Xie, Z. L. Wang, *ACS applied materials & interfaces* **2014**, *6*, 3031-3038.

[39] K. Sitapati, R. Krishnan, *IEEE Transactions on industry applications* **2001**, *37*, 1219-1226.

[40] M. Niroomand, H. Foroughi, *Journal of applied research and technology*, **2016**, *14*, 259-267.

[41] S. P. Beeby, R. Torah, M. Tudor, P. Glynne-Jones, T. O'donnell, C. Saha, S. Roy, *Journal of Micromechanics and microengineering* **2007**, *17*, 1257.

[42] T. O'Donnell, C. Saha, S. Beeby, J. Tudor, *Microsystem Technologies* **2007**, *13*, 1637-1645.

[43] C. W. T. McLyman, *Transformer and inductor design handbook*, CRC press **2017**.

[44] B. Yang, C. Lee, W. Xiang, J. Xie, J.H. He, R.K. Kotlanka, S.P Low, H. Feng, *Journal of Micromechanics and Microengineering*, **2009**, *19*, 035001.

[45] Z. Yang, J. Zu, *Energy Conversion and Management* **2016**, *122*, 321-329.

[46] K. Fan, J. Chang, F. Chao, W. Pedrycz, *Energy Conversion and Management* **2015**, *96*, 430-439.

[47] J. Wei, L. Duan, *ASME 2015 Conference on Smart Materials, Adaptive Structures and Intelligent Systems, American Society of Mechanical Engineers* **2015**, V002T07A005-V002T07A005.

[48] A. Erturk, D. J. Inman, *Smart materials and structures* **2009**, *18*, 025009.

[49] P. Pillatsch, E. M. Yeatman, A. S. Holmes, *Smart Materials and Structures* **2013**, *23*, 025009.

[50] W. S. Trimmer, *Sensors and actuators* **1989**, *19*, 267-287.

[51] (a) W. J. Choi, Y. Jeon, J.-H. Jeong, R. Sood, S. G. Kim, *Journal of Electroceramics* **2006**, *17*, 543-548; (b) H. Hosaka, K. Itao, S. Kuroda, *Micro Electro Mechanical Systems*, *1994, MEMS'94, Proceedings, IEEE Workshop on, IEEE* **1994**, 193-198.

[52] S. Shahab, S. Zhao, A. Erturk, Performance Comparison of Soft and Hard Piezoelectric Ceramics and Single Crystals for Random Vibration Energy Harvesting, *Energy Technology*, **2017**, online.

WILEY-VCH

Accepted Manuscript

This article is protected by copyright. All rights reserved.

10.1002/ente.201800151

WILEY-VCH

FULL PAPER

Three key types of micro-generators (energy harvesters), namely electromagnetic (EMREHs), piezoelectric resonant (PRREHs) and piezoelectric non-resonant rotational energy harvesters (PNRREHs) are discussed and compared in terms of device dimensions and operation frequencies. Theoretical models are established to calculate maximum achievable output power as a function of device dimension and operating frequency. Scaling laws are established for each type based on the theoretical models. The EMREHs have a strong scaling effect both on device dimension (as L^5) and on operating frequency (as ω^2), whereas the PNRREHs are less so ($L^{2.5}\omega^{0.5}$). PRREHs are narrowband and ideal for constant excitation frequency cases. This study provides a guideline for selection and design of rotational energy harvesters for different device dimensions and operating frequencies.

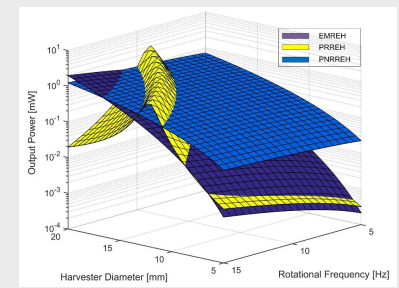

*Author(s), Corresponding Author(s)**

Hailing Fu* and Eric M. Yeatman

Page No. – Page No.

Title: Comparison and Scaling Effects of Rotational Micro-Generators using Electromagnetic and Piezoelectric Transduction

Accepted Manuscript

This article is protected by copyright. All rights reserved.